GEOPHYSICS, VOL. 60, NO. 3 (MAY-JUNE 1995); P. 692-701, 10 FIGS.

High-resolution crosswell imaging of a west Texas carbonate reservoir: Part 3-Wavefield separation of reflections

James W. Rector III*, Spyros K. Lazaratos‡, Jerry M. Harris§ and Mark Van Schaacks

ABSTRACT

Using crosswell data collected at a depth of about 3000 ft (900 m) in West Texas carbonates, one of the first well-to-well reflection images of an oil reservoir was produced. The P and S brute stack reflection images created after wavefield separation tied the sonic logs and exhibited a vertical resolution that was comparable to well log resolution. Both brute stacks demonstrated continuity of several reflectors known to be continuous from log control and also imaged an angular unconformity that was not detected in log correlations or in surface seismic profiling. The brute stacks, particularly the S-wave reflection image, also exhibited imaging artifacts.

We found that multichannel wavefield separation filters that attenuated interfering wavemodes were a critical component in producing high-resolution reflection images. In this study, the most important elements for an effective wavefield separation were the time-alignment of seismic arrivals prior to filter application and the implementation of wavefield-separation filters in multiple domains, particularly in common offset domain. The effectiveness of the multichannel filtering was enhanced through the use of extremely fine wellbore sampling intervals. In this study, 2.5 ft (0.76 m) vertical sampling intervals for both source and receiver were used, whereas most previous crosswell data sets were collected with much coarser sampling intervals, resulting in spatial aliasing and limiting the utility of the data for reflection processing. The wavefield separation techniques employed in this study used data volumes and associated filtering operations that were several orders of magnitude larger than those encountered in conventional VSP data analysis.

INTRODUCTION

Several authors have recently proposed using crosswell reflection arrivals to image the subsurface between boreholes (Lazaratos et al., 1991; Stewart and Marchisio 1991). Crosswell imaging with reflections holds several advantages over more conventional transmission tomography techniques. First and foremost, reflections provide an image of horizons *at and below the well base*. Transmission tomography images the interwell plane *above* the well base and suffers from coverage artifacts near the bottom of the survey. Second, a transmission traveltime tomogram is critically dependent upon the angular aperture of rays transecting an interwell zone. Aperture variations and/or angular dependence of velocity (anisotropy) can produce image distortion. Reflection images are less dependent upon angular aperture. In fact, high quality seismic reflection images with good lateral and vertical resolution can be constructed from normal incidence raypaths with little angular aperture (e.g., surface reflection profiling).

Our approach to crosswell imaging can be compared and contrasted with diffraction tomography. In diffraction tomography, the secondary or scattered field is used to produce quantitative estimates of interwell velocity fields (Wu and Toksoz, 1987; Harris, 1987; Pratt and Goulty, 1991). The inhomgeneities are often assumed to be weak (allowing the use of the Born approximation) and the scattered field is generally assumed to consist of all arrivals other than the primary direct arrival. An example of diffraction tomography applied to acoustic tank crosswell data was

Manuscript received by the Editor March 17, 1994; revised manuscript received December 8, 1994.
*Engineering Geoscience, University of California-Berkeley, Berkeley, CA 94720.
‡Formerly Department of Geophysics, Stanford University; currently TomoSeis Inc., 1650 W. Sam Houston Pkwy. N., Houston, TX 77043-3115.
§Department of Geophysics, Stanford University, Stanford, CA 94305.

discussed by Pratt and Goulty (1991). Although some features of the interwell velocity field were resolved with diffraction tomography, image distortions and obvious artifacts were also present. In our approach to crosswell imaging we are concerned with imaging only the primary reflections, which are a small subset of the entire scattered wavefield.

To isolate the primary reflections from the rest of the wavefield, we apply extensive wavefield separation filtering *prior* to stacking. As in surface reflection profiling, identifying reflections in crosswell data prior to stacking is extremely important for optimizing statics and estimating stacking or migration velocities (Lazaratos et al., 1995). Wavefield separation filtering of crosswell reflection data is an extension of VSP processing where upgoing reflections are separated from downgoing (direct) arrivals (Hardage, 1985). Crosswell reflections can be separated from the rest of the wavefield using multichannel filters applied to common source gathers (CSG), common receiver gathers (CRG), and common offset gathers (COG) (Rector et al., 1994). These gathers are analogous to those used in surface seismic imaging except that the independent variable in a crosswell data set is depth rather than horizontal position along the earth's surface. In this study, wavefield separation was used to extract eight primary reflection data subsets from the raw data. The reflection subsets were described by their direction of travel (upgoing or downgoing), the body wave mode (S or P) , and the reflection point location within the image plane (nearer to the source well or the receiver well).

We conclude this paper by creating two *P* and S brute stacks by combining the wavefield-separated data. Although the brute stacks exhibit reflection arrivals that tie the sonic log, there are still imaging artifacts, particularly near the midpoint between the two wells. In a companion paper, Lazaratos et al. (1995), techniques to attenuate these artifacts are implemented, resulting in high quality crosswell reflection images having a vertical resolution comparable to well logs.

DATA ACQUISITION AND INITIAL DATA ANALYSIS

The area chosen to evaluate our approach to reflection imaging was a west Texas carbonate reservoir targeted for a CO_2 flood pilot study (Harris et al. 1995). The site was ideal because the rocks consisted of high Q carbonates through which very high frequencies were expected to propagate and the stratigraphic layering was known to be relatively flat (Harris et al., this issue).

The crosswell data acquisition geometry for this study is discussed in Harris et al. (this issue). For the purposes of wavefield separation, the key acquisition parameter was the 2.5 ft (0.76 m) depth sampling of source and receiver positions. Fine depth sampling was required to avoid spatial aliasing of high-frequency tube waves, S-waves, and P-to-S converted waves. In a typical CRG or CSG at this site, the tube waves spatially overlap (two arrivals exhibiting the same value in f-k space) with P-wave reflection arrivals at frequencies above 1600 Hz and spatially overlapped S-wave reflections above 1100 Hz. Although we could not spatially sample the data finely enough to avoid some amount of aliasing and resulting overlap, multiple wraps of tube waves around the Nyquist wavenumber were avoided. In most previously recorded crosswell surveys, spatial sampling intervals were 10 to 20 ft (3 to 6 m), resulting in severe spatial aliasing problems and reducing the potential effectiveness of multichannel filters in separating arrivals.

WAVEFIELD SEPARATION

We focused on the wavefield separation of S-wave reflections because they were more prominent and easier to extract and characterize than the P-wave reflections for this data set. One possible explanation for this phenomena is provided by the piezoelectric source radiation pattern and the hydrophone reception pattern (Van Schaack et al., 1992), which predicts that for our survey geometry, the ratio of S-wave reflected arrivals to S-wave direct arrivals will be larger than the same ratio for P-wave arrivals. Besides radiation pattern considerations, the S-wave reflections are easier to extract from the total wavefield because they do not have to contend with any transmitted interference. The P-wave reflections temporally overlap with transmitted interference such as the S-wave direct arrival, S-to-P transmitted conversions, and P-to-S transmitted conversions. By contrast, S-wave reflections overlap only with other reflections and tube waves. Since transmitted arrivals are usually larger than reflected arrivals, the other reflections that interfere with S-wave reflections have lower amplitudes than the transmitted arrivals that interfere with P-wave reflections. It should be mentioned that the velocities of these carbonates were high enough to avoid the production of conical waves (Meredith, 1990). In lower velocity rocks, the presence of conical waves could make extracting S-wave reflections more difficult.

We illustrate the wavefield separation processing by extracting S-wave reflections, consisting of upgoing and downgoing reflections coming from points near the source well, using a common receiver gather (Figure 1) from a depth of 2880 ft (880 m). The desired reflections, labeled as D in Figure 1, have moveouts opposite in sign from the direct arrival moveout. The wavefield separation process for these arrivals is the left-hand branch of the flow chart shown in Figure 2.

The first step in the wavefield separation process was to sort the data into common offset gathers. In common offset space, the direct arrival moveout is nearly zero, exhibiting a moveout that is dependent upon velocity variations rather than path length changes (Rector, et al., 1994), and upgoing and downgoing reflections can be separated from the direct arrival for all traces (Pratt and Goulty, 1991). Figure 3 shows the common offset data corresponding to the source/receiver pairs in Figure 4. The moveout of the *P* and S direct arrivals is nearly zero, and both the *P* and S direct arrival times mimic the variation of velocity with depth seen in the sonic log. The low velocity reservoir interval between 2850 and 2950 ft (870 m and 901 m) can be seen as an increase in both *P*- and S-wave direct arrival traveltime. The S-wave reflections can be identified as steeply dipping events [with an apparent velocity of around 6000 ft/s (1830 m/s)] following the S direct arrival.

The second step in the wavefield separation process was to align the S direct arrival. This step is similar to direct arrival alignment in VSP processing (Hardage, 1985). The arrival is aligned (using time picks or modeled traveltimes) to concentrate the arrival energy in a small spatial bandwidth

around $k = 0$. Then the aligned energy can be attenuated using a narrow multichannel filter, preserving all but a small portion of the 2-D spectrum. Figure 5 illustrates the effect of arrival alignment on the f-k spectrum. Before alignment, the direct arrival is spread over a relatively large portion of the f-k spectrum. After alignment, the direct arrival is concentrated in a narrow spatial frequency range around $k = 0$.

The first multichannel filter applied to the data (WF #l in Figure 2) consisted of:

1) scaling each trace in a 4 ms window around the direct arrival,
2) performing an 1 l-trace mean mix of the data,
3) subtracting the mixed data from the premixed, aligned data.

Subsequent multichannel filters omitted step (a). Tests were performed with different formulations for multichannel filtering, including mean, median and f-k fan filters, and there was little visual difference in the results. We selected the mean filter because it was the fastest to run. Speed was important because the wavefield separation required for this data set was comparable to the wavefield separation that would be required for 7,500 offset VSP's. Figure 6a shows the common receiver data (dealigned) after attenuation of the S-direct arrival. Note that the direct arrival is substantially attenuated and both the upgoing and downgoing S-wave reflections are easier to identify. We can also observe some interesting characteristics of the wavefield that cannot be detected in the raw data. For example, the event labeled as H in Figure 1 is shown to originate from the P-to-S converted arrival rather than the S-direct arrival. Therefore this arrival is probably a double conversion (P-to-S-to-P) rather than a simple S-to-P conversion.

The next stage of the wavefield separation process was to attenuate receiver well reflections (WF #2) and enhance source well reflections (WF #3). Figure 6b shows the common receiver data after WF #2 (and dealingment). Note that the crossing S-wave reflections coming from points near the receiver well have been substantially attenuated, because S-wave reflections coming from near the receiver well have a moveout similar to the S direct arrival. Note also that the effectiveness of the filter in removing crossing arrivals deteriorates as we move later in time away from the direct

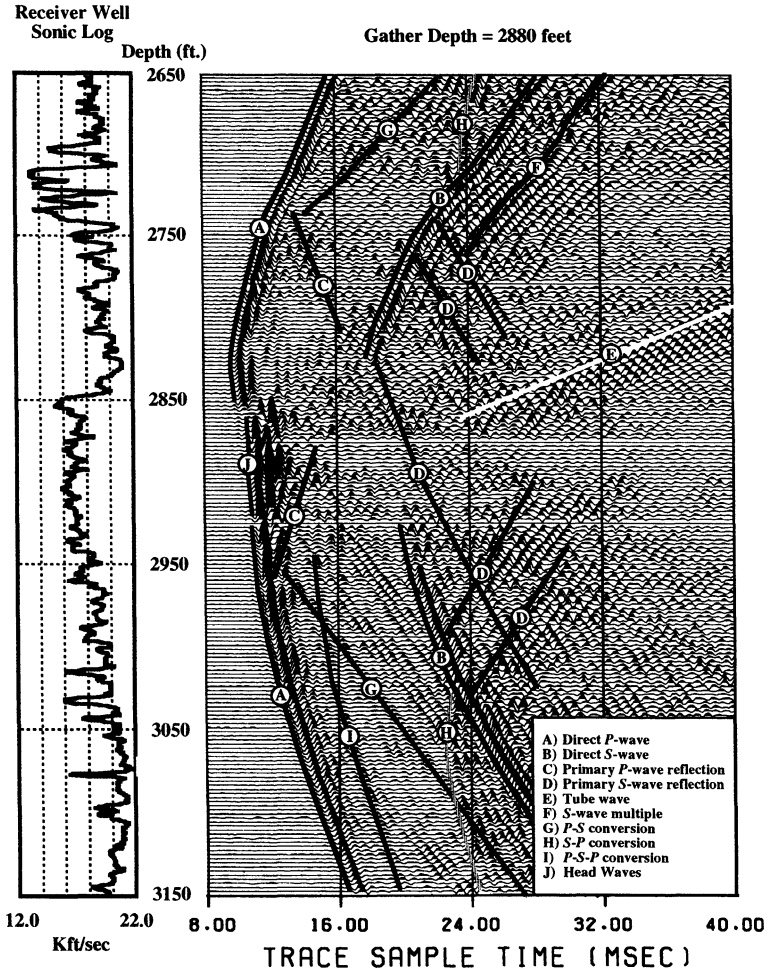

FIG. 1. An unprocessed field gather and velocity log from the receiver well with many arrivals highlighted and labeled. The common receiver gather was collected with a hydrophone located at 2880 ft (880 m) and source positions ranging from 3150 ft to 2650 ft (960 m to 810 m). The trace interval was 2.5 ft (.76 m).

arrival, because the direct arrival moveout becomes a less accurate model for the receiver well reflection moveout. Figure 6c shows the data after WF #3. Both the upgoing and downgoing reflections are cleaner and the reflections still terminate near the direct arrival even though a trace mix was used rather than a median filter.

At this stage in the processing we applied a deterministic deconvolution filter to the reflection arrivals much like the downwave deconvolution processing performed in VSP (Hardage, 1985). The deterministic operator was derived on a trace-by-trace basis from the aligned and enhanced S-direct arrival. The alignment and enhancement was performed in common offset space using WF #1 to provide maximum rejection of S-wave reflections. Figure la shows the common receiver wavefield resulting from this processing. In addition to the direct arrival there are upgoing and downgoing arrivals that have moveouts similar to the primary reflections. These arrivals may be the up/down multiples described in Rector et al. (1994) because, unlike primaries, they terminate before reaching the direct arrival. Figure 7b shows the enhanced S-direct arrival after deterministic deconvolution. Besides compressing the wavelet (the compressed wavelet is about 0.6 ms or roughly the sweep bandwidth), the up/down multiples have been attenuated.

The final stage of the wavefield separation process was to decompose the deconvolved reflections into upgoing and downgoing components (we also muted the data at the S direct arrival time). The upgoing and downgoing reflections were obtained thmugh simple *f-k* pie-slice filters. Figures 8a and 8b show the upgoing and downgoing reflection components after applying the *f-k* filters. Comparing Figure 8 with Figure 1, it is apparent that it is much easier to identify the reflections after applying the wavefield separation processing.

The wavefield separation processing for this data set was a computer intensive operation. Considering the number of gathers (roughly 200 in each domain) and the number of processes, the volume of data processed was comparable to processing over 7500 offset VSPs. Once the Row was developed, the actual data processing took about two days to complete using *ProMAX* processing software on a small (less than 3 Mflop) workstation. Even though *ProMAX* was designed for surface seismic data, we found that it could be modified to handle crosswell data.

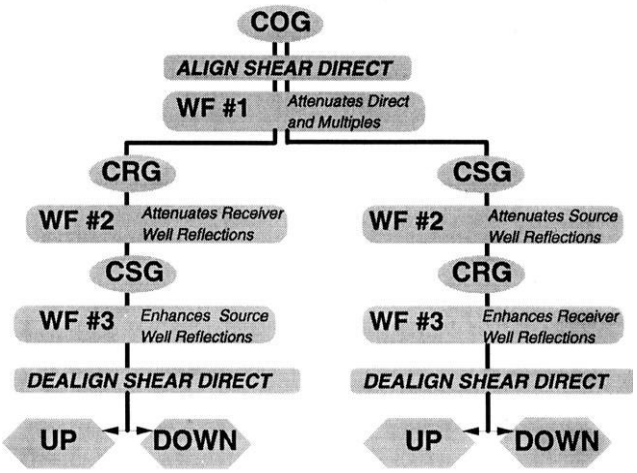

FIG. 2. Wavefield separation processing flow devised for this crosswell data set. COG, CSG, and CRG refer to sorting operations that transform the input sort into common offset, common source, and common receiver gathers, respectively. WF stands for application of a multichannel filter.

BRUTE STACK

After wavefield separation and deconvolution, the reflection wavefields were imaged using a modified VSP-CDP algorithm [Wyatt and Wyatt (1981)]. The VSP-CDP algorithm was modified to allow imaging of both upgoing and downgoing reflections. The VSP-CDP algorithm was used instead of a prestack migration to reduce the spatial smearing of artifacts associated with limited aperture and coherent noise (Lazaratos et al., this issue). The *P*- and S-wave velocity models used for mapping were layered models derived from I-D tomographic inversions of direct arrival time picks (Van Schaack et al., 1992). Figure 9 shows the tomogram velocities superimposed on the smoothed sonic logs.

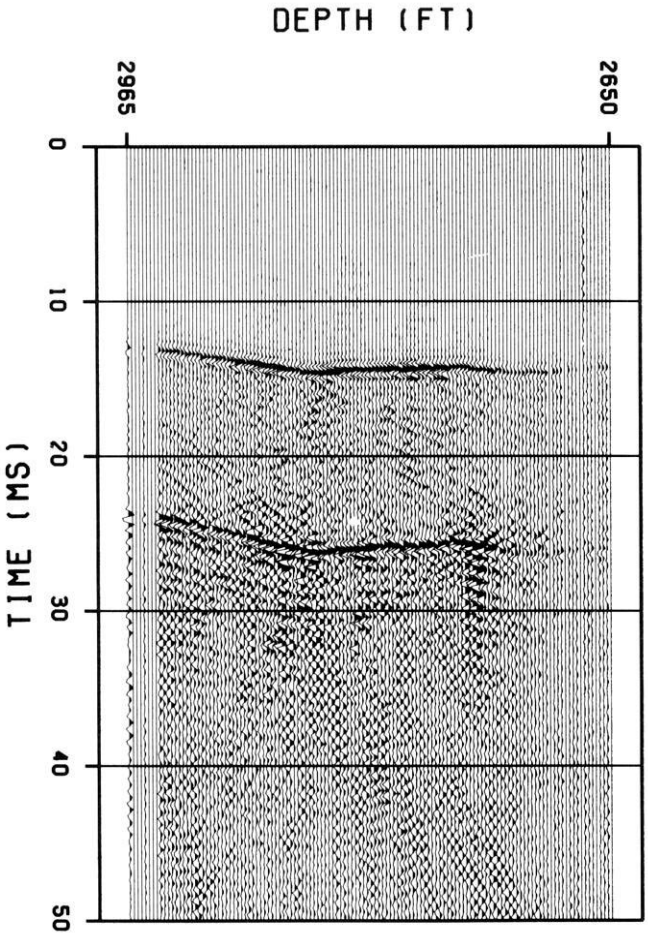

FIG. 3. Common offset gathers corresponding to source/receiver wireline depth separations of +90 ft (27 m) [receivers 90 ft (27 m) deeper than sources]. The first large arrival is the P-direct arrival. The second large arrival is the S-direct arrival.

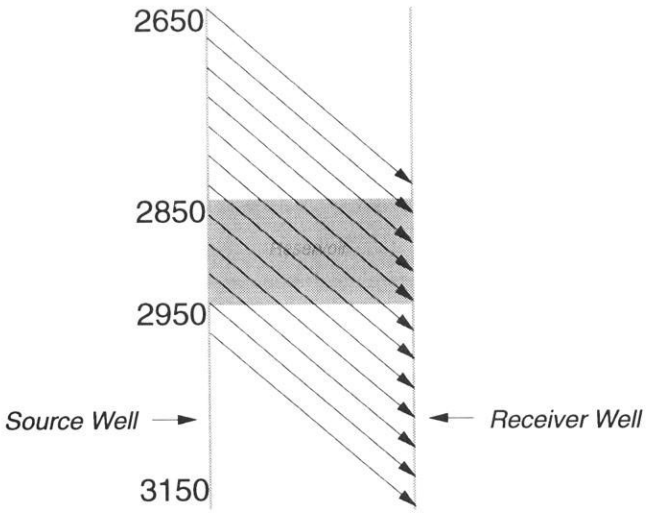

FIG. 4. Straight raypaths corresponding to the gathers shown in Figure 5.

Once all individual gathers (common source, common receiver, upgoing, downgoing, *P-to-P*, and S-to-S) were mapped, we stacked the mapped gathers to produce *P*- and S-wave reflection images. We call the images brute stacks because they are produced by a one-step mapping and stacking procedure, without any post-map velocity analysis, statics, or incidence angle filtering (Lazaratos et al., this issue). The brute stacks are shown in Figure 10a (S) and Figure 10b (P) along with the source and receiver well sonic logs. Since an S-wave sonic was not run on the receiver well, we display the *P-wave* sonic for the receiver well on the S-wave reflection image. Downgoing reflections were used to image the depth range from 2700 ft to 3000 ft (800 m to 900 m) and upgoing reflections were used to image depths below 3000 ft (900 m). These cutoff depths were chosen based on the quality of the stacked output. The downgoing stack was considered to have the highest signal-to-noise ratios above 3000 ft (900 m) while the upgoing stack was considered to have the highest signal-to-noise ratios below 3000 ft (900 m).

The brute stacks have very high vertical resolution. The reflection wavelengths were as small as 5 ft (1.5 m) for the

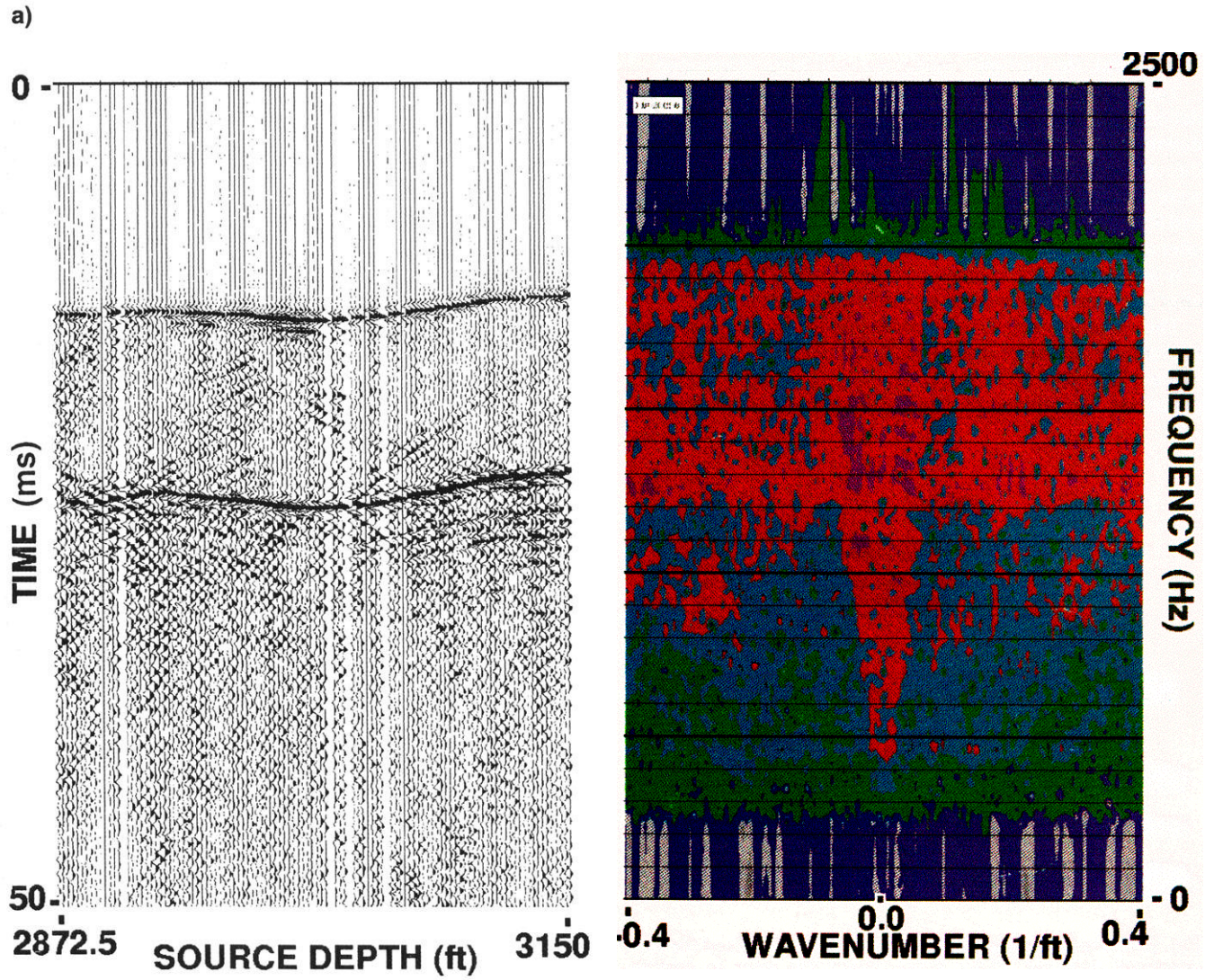

FIG. 5. (a) Common offset gather and corresponding ***f-k*** spectrum. (b) Common offset gather with the S-direct arrival aligned and the corresponding ***f-k*** spectrum.

S-wave image, producing a vertical bed resolution of a little more than 1 ft (0.3 m). The brute stacks exhibit good ties with the sonic logs at the wells, but degrade in quality toward the midpoint between the two wells. One explanation for the degradation toward the middle of the image is the wavefield separation techniques used in WF #2 and WF #3. As discussed previously, these filters are optimized for reflections occurring in time near the direct arrival. Reflections near the midpoint between the two wells are not optimally separated from other interference. However, there are some reflectors, particularly on the ***P*** image, that are continuous from well to well. The S image has higher resolution (shorter wavelengths) than the ***P*** image because for these data, the frequency content of the S-waves was similar to that of the P-waves.

Both the ***P*** and S brute stacks exhibit several continuous reflectors, but perhaps more interesting is an angular unconformity at about 3050 ft (920 m) that is imaged by both ***P-wave*** and S-wave reflections. The interpretation of this angular unconformity is discussed in more detail in Harris et al. (this issue) and Lazaratos et al. (this issue). There are also obvious artifacts in the brute stacks, particularly in the S-wave image, and the coherency of the S-wave image is lower than the coherency of the ***P-wave*** image. This is somewhat surprising when considering the quality of the raw data, which showed much higher amplitude S-wave reflections than ***P-wave*** reflections. The causes for the image artifacts and a methodology for their attenuation are discussed in Lazaratos et al. (this issue).

CONCLUSIONS

To produce reliable and meaningful crosswell reflection images it is necessary to first extract the primary reflections from the unwanted interference modes. This process is extremely important in crosswell reflection imaging because there are so many types of elastic interference modes that are time-coincident with the primary reflections. The coincidence of the noise and the reflections means that multichannel filters are required to remove the interference.

The field data examined in this study were acquired with a 2.5 ft (0.76m) sampling interval to avoid significant spatial

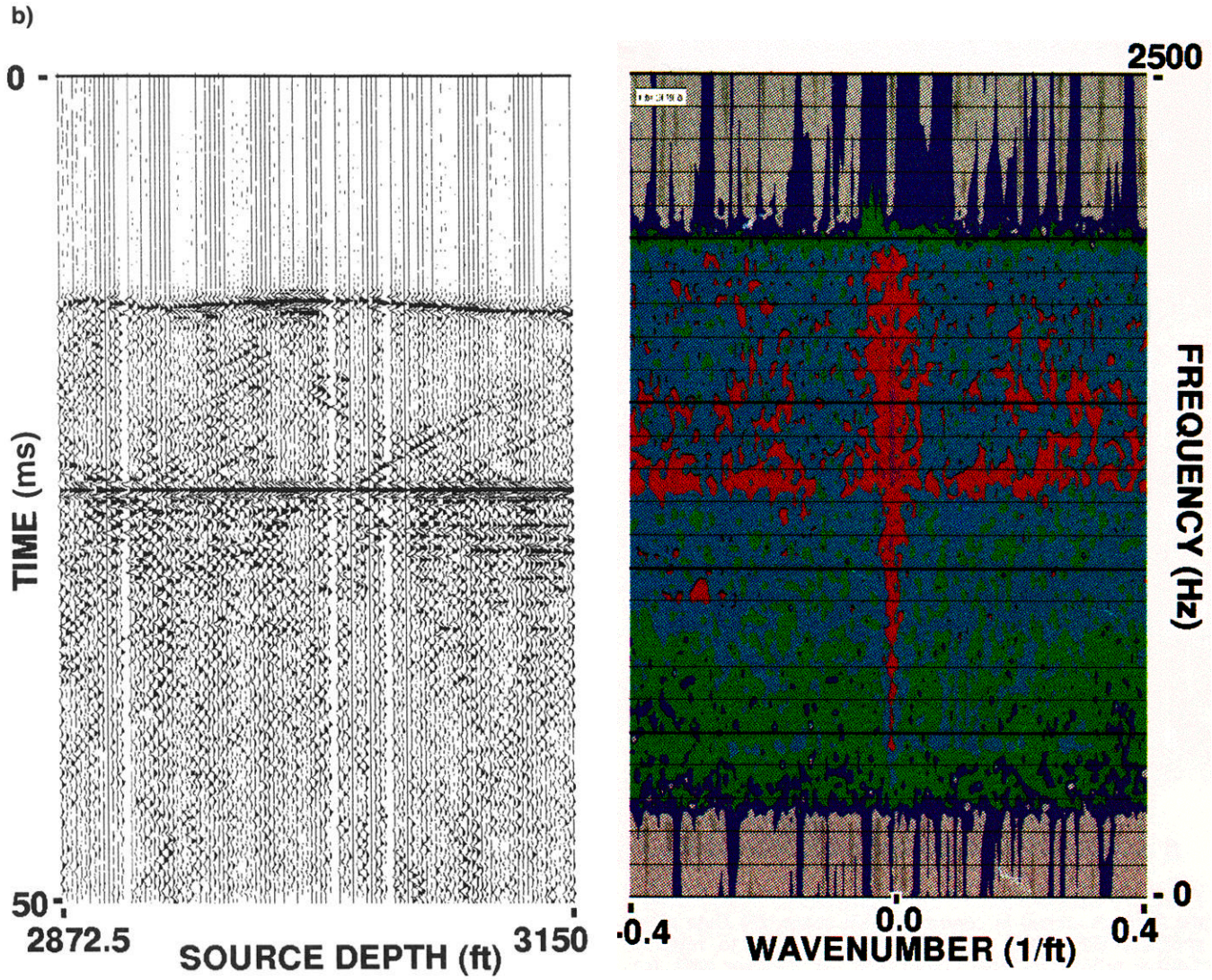

FIG. 5. (continued)

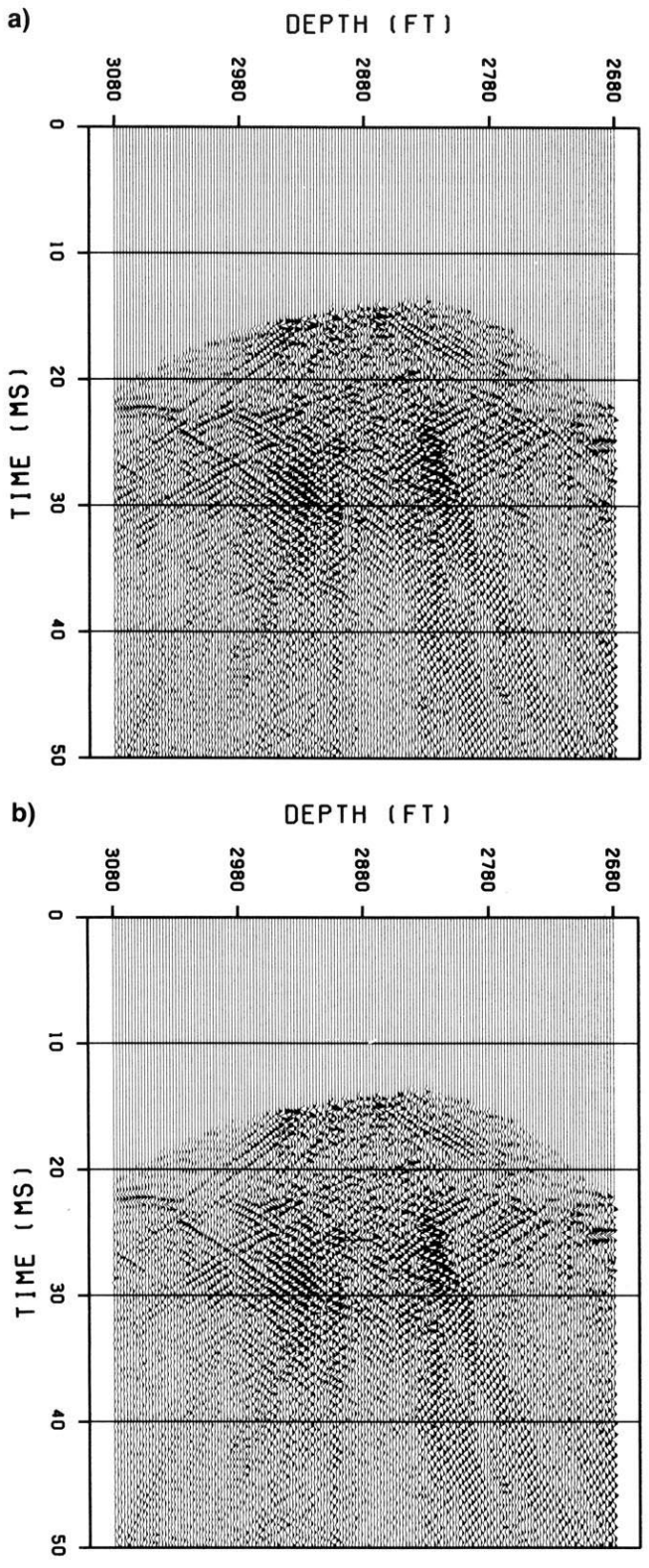

FIG. 6. (a) Data of Figure 1 after applying WF #1 to remove the S-direct arrival in common offset space. (b) Data after applying WF #2 in common receiver space to remove S-wave reflections from points near the receiver well. (c) Data after applying WF #3 to enhance reflections coming from near source well.

aliasing of the slowest noise mode (the tube wave) and to improve the wavefield separation capability of multichannel filters. Most crosswell data sets acquired prior to this study could not be effectively processed for reflections because the spatial sampling intervals were too coarse to effectively utilize multichannel filters for wavefield separation. We found that the arrival alignment and the use of multiple sorting domains (particularly common offset space) for multichannel filtering were key elements for an effective wavefield separation. The actual filtering algorithm was secondary. The volume of data processed and the number of operations performed were two and four ***orders of magnitude*** greater, respectively, than a typical VSP.

The brute stacks demonstrated the utility of crosswell reflection imaging. The reflection images had a vertical resolution that was comparable to well-log resolution. The brute stacks also illustrated an angular unconformity that was not detected in either log correlations or in surface reflection profiling. The brute stack reflection images near the boreholes tied with sonic logs, but the reflection image quality degraded as the reflection points moved toward the center of the interwell region. The image degradation is consistent with the direct-arrival-based wavefield separation and deconvolution used in this study, which work best for reflections near the direct arrival. A wavefield separation that is more model based may improve the quality of the reflection images toward the midpoint. The S brute stack exhibited fewer coherent events than the ***P*** brute stack even though the wavefield-separated S-wave reflections input to the brute stack appeared to be a higher quality than the ***P-wave*** reflections. These effects are investigated and the

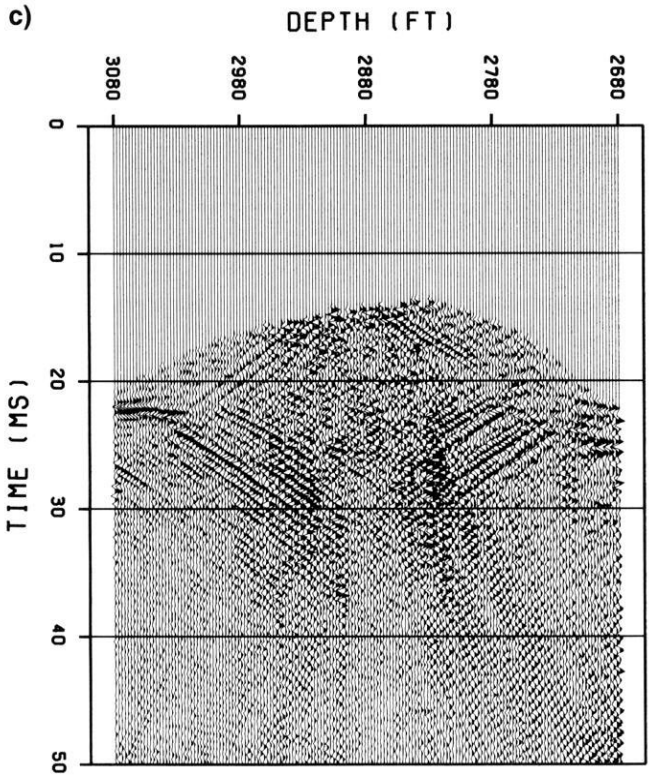

FIG. 6.

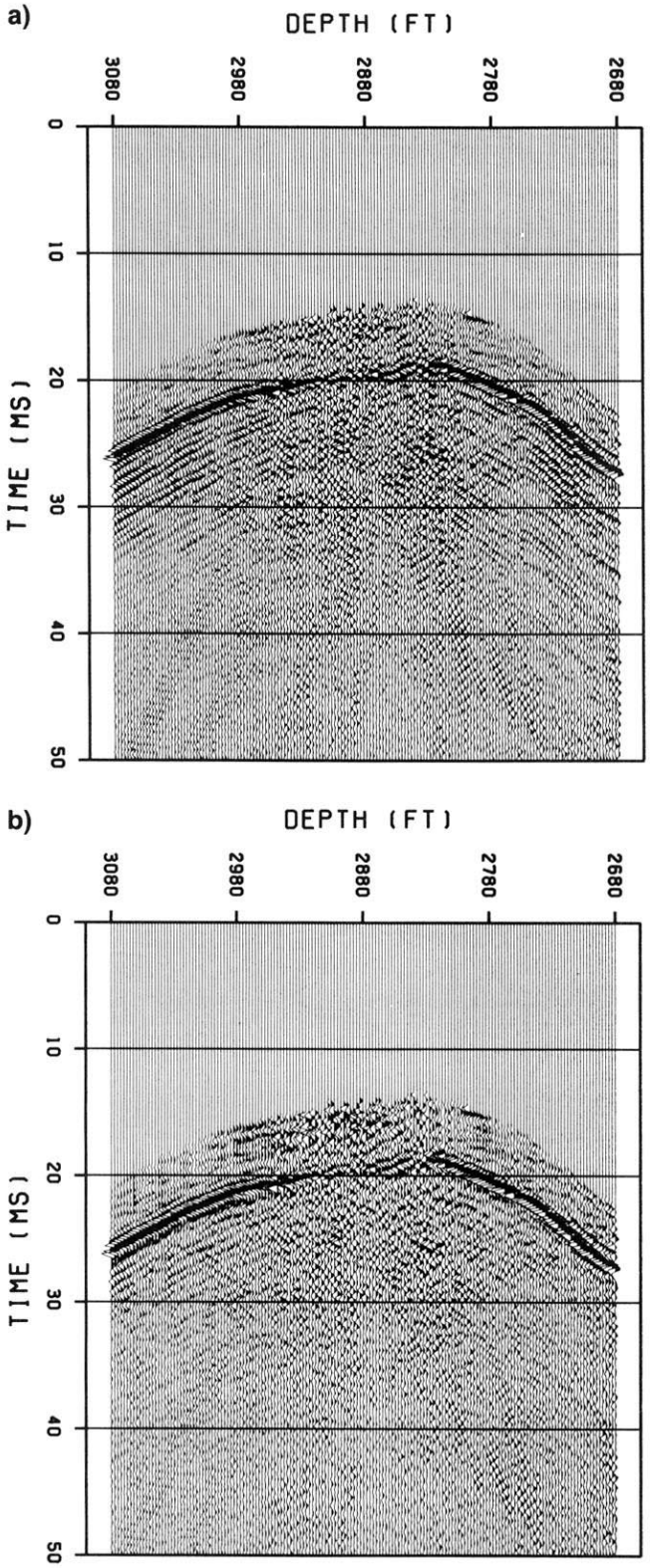

FIG. 7. (a) Enhanced S-direct arrival wavefield. (b) Data after deterministic deconvolution of the data in Figure 7a.

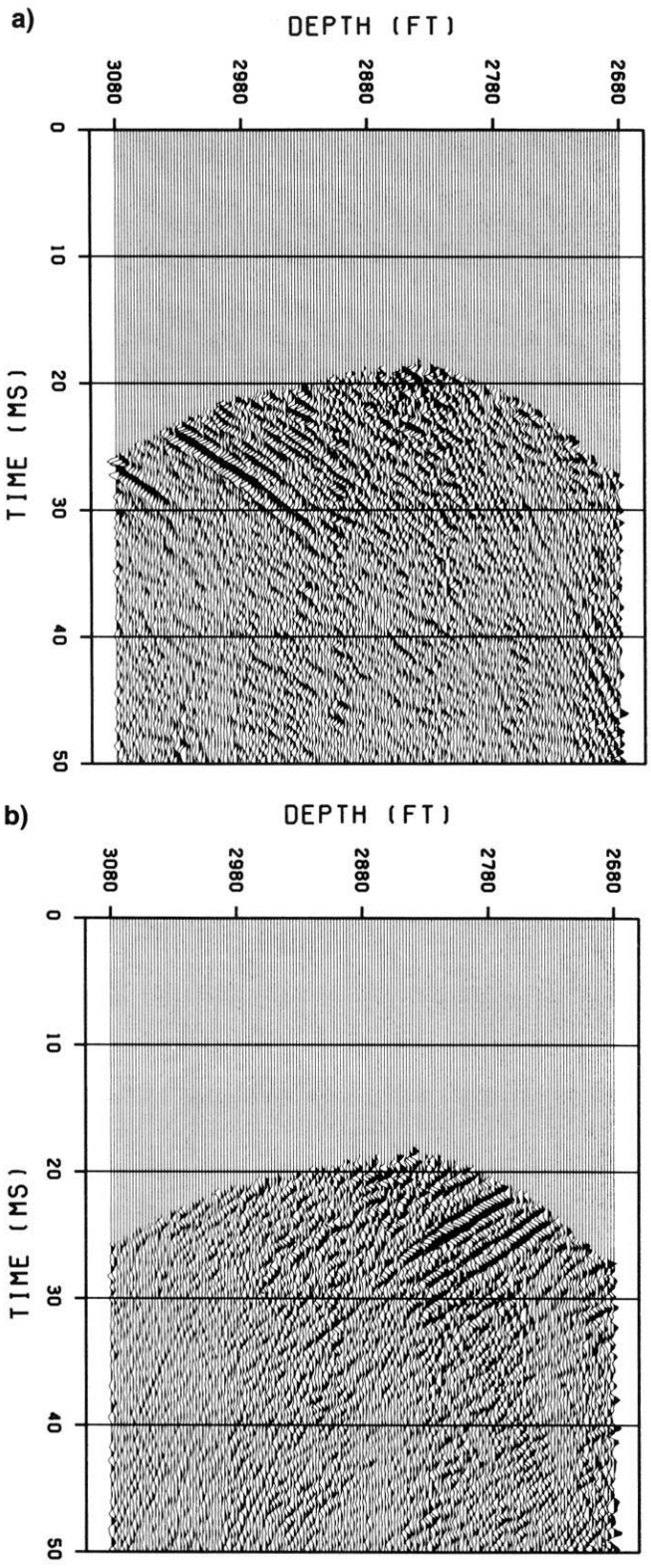

FIG. 8. (a) Primary upgoing S-wave reflections obtained from Figure 1 after wavefield separation and deterministic deconvolution. (b) Same as Figure 8a only downgoing. These wavefields are used as input to the brute stack (Figure 10) and subsequent imaging discussed in Lazaratos et al. (1995, this issue).

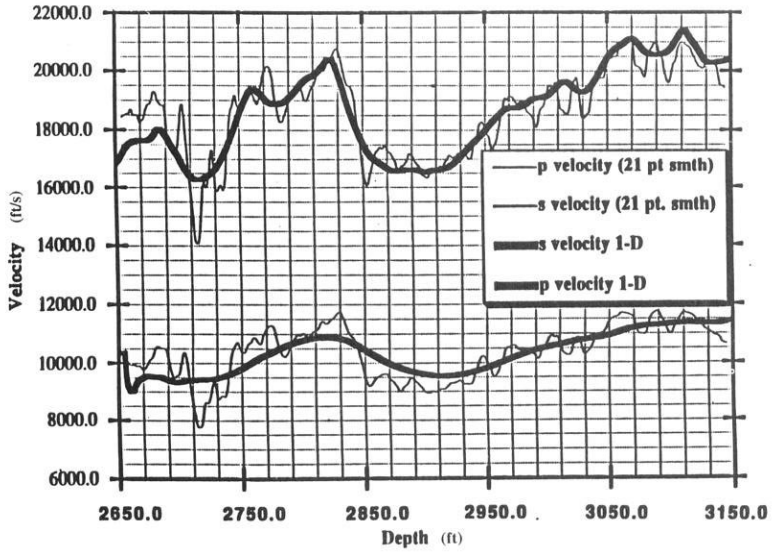

FIG. 9. Velocity models derived from tomograms for reflection imaging (thick lines) superimposed on smoothed sonic logs (thin lines).

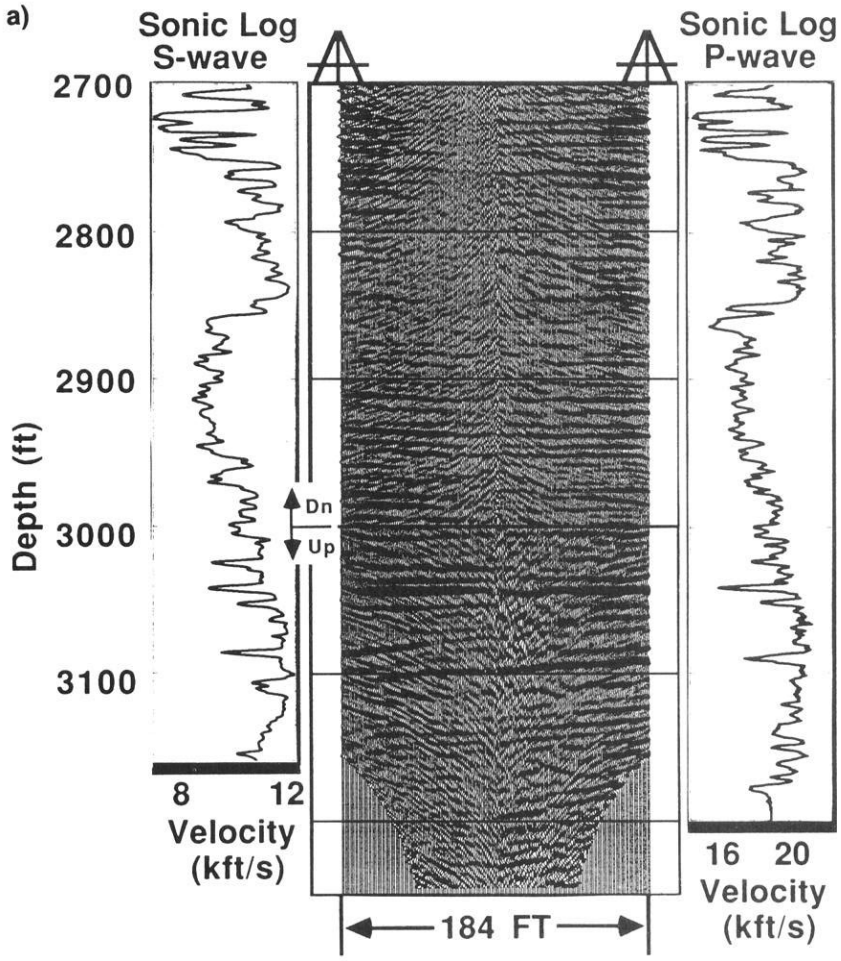

FIG. 10. (a) *S* brute stack. (b) ***P*** brute stack.

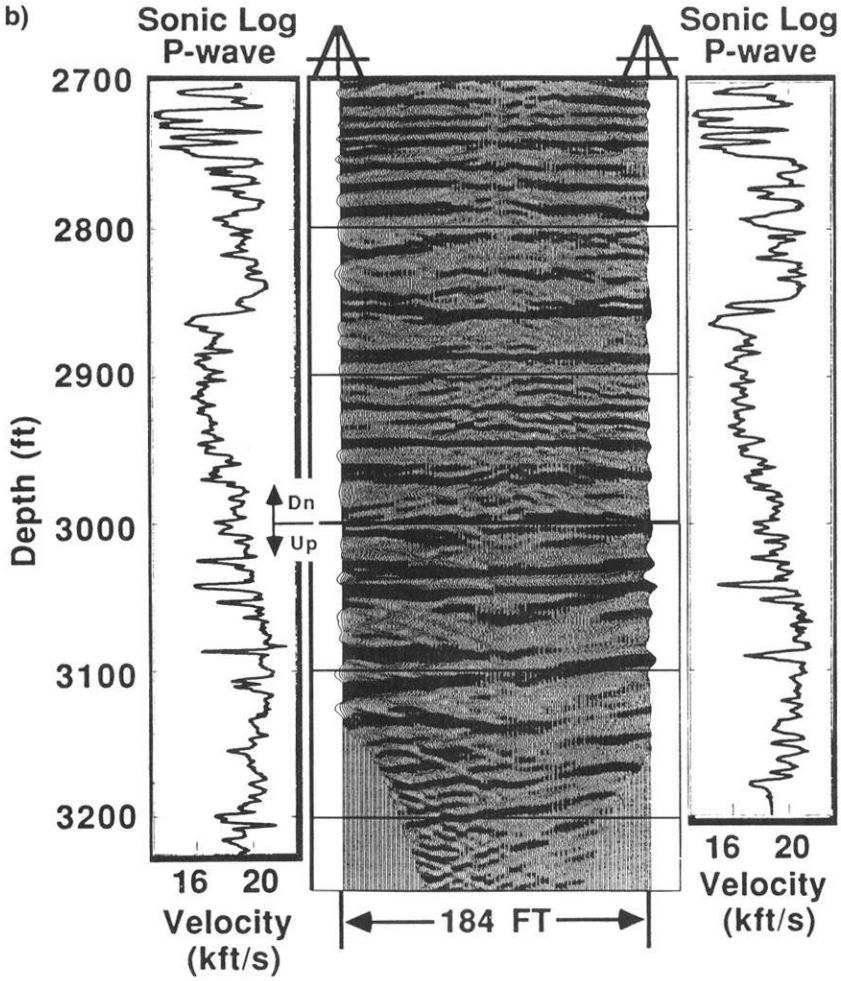

FIG. 10. (continued)

image quality is dramatically improved with post-imaging reflection processing. This processing is discussed in Lazaratos et al. (this issue).

ACKNOWLEDGMENTS

The authors are grateful to the Gas Research Institute (GRI) and to Chevron Petroleum Technology Corporation for providing the field site and co-sponsoring this research. Insightful comments by the Associate Editor and two reviewers were very helpful in producing the revised manuscript.

REFERENCES

Hardage, B. A., 1985, Vertical seismic profiling--Part 1 Principles: Pergammon Press, 2nd Edition.

Harris, I. M., Nolen-Hoeksema, R., Langan, R. T., Lazaratos, S. K., Van Schaack, M., and Rector, J. W., 1995, High-resolution crosswell imaging of a west Texas carbonate resevoir: Part I-Project summary and interpretation, Geophysics, **60,** 667-681.

Harris, J. M., 1987, Diffraction tomography with arrays of discrete sources and receivers: IEEE Trans. Geosci. and Remote Sensing, Vol GE-25, 4, 448-455.

Lazaratos, S. K., Rector, I. W., Harris, J. M., 1991, High resolution cross-well reflection imaging: 61st Ann. Internat. Mtg., Soc. Expl. Geopbys., Expanded Abstracts, 350-353.

Lazaratos, S. K., Harris, J. M., Rector, J. W., and Van Schaack, M., 1995, High-resolution crosswell imaging of a west Texas carbonate reservoir: Part 4.Reflection imaging, Geophysics, **60,** 702-711.

Meredith, J., 1990, Numerical and analytical modeling of downhole seismic sources: The near and far field: Phd. Thesis, Massachusetts Institute of Technology.

Pratt, R. G., and Goulty, N. R., 1991, Combining wave-equation imaging with traveltime tomography to form high resolution images from crosshole data: Geophysics, **56,** 208-225.

Rector, J. W., Lazaratos, S. K., Harris, J. M., and Van Schaack, M., 1994, Multidomain analysis and wavefield separation of cross-well seismic data: Geophysics, **59,** 10-20.

Stewart, R. R., and Marchisio, G., 1991, Crosswell seismic imaging using reflections: 61st Ann. Internat. Mtg., Soc. Expl. Geophys., Expanded Abstracts, 375-378.

Van Schaack, M., Harris, I. M., Rector, J. W., and Lazaratos, S. K., 1992, High resolution imaging of a west Texas carbonate reservoir: Part 2, Traveltime tomography: 62nd Ann. Internat. Mtg., Soc. Exp,. Geophys., Expanded Abstracts, 40-44.

Wu, R., and Toksoz, M. N., 1987, Diffraction tomography and multisource holography applied to seismic imaging: Geophysics, **52,** 11-25

Wyatt and Wyatt, 1981, Determination of subsurface structural information using the vertical seismic profile: Presented at the 51st Ann. Internat. Mtg., Soc. Expl. Geophys.